# Three applications of path integrals: equilibrium and kinetic isotope effects, and the temperature dependence of the rate constant of the [1,5] sigmatropic hydrogen shift in (Z)-1,3-pentadiene

Tomáš Zimmermann[1] and Jiří Vaníček[1, *]

[1]*Laboratory of Theoretical Physical Chemistry, Institut des Sciences et Ingénierie Chimiques,*
*École Polytechnique Fédérale de Lausanne (EPFL), CH-1015 Lausanne, Switzerland*
(Dated: April 2, 2010)

Recent experiments have confirmed the importance of nuclear quantum effects even in large biomolecules at physiological temperature. Here we describe how the path integral formalism can be used to describe rigorously the nuclear quantum effects on equilibrium and kinetic properties of molecules. Specifically, we explain how path integrals can be employed to evaluate the equilibrium (EIE) and kinetic (KIE) isotope effects, and the temperature dependence of the rate constant. The methodology is applied to the [1,5] sigmatropic hydrogen shift in pentadiene. Both the KIE and the temperature dependence of the rate constant confirm the importance of tunneling and other nuclear quantum effects as well as of the anharmonicity of the potential energy surface. Moreover, previous results on the KIE were improved by using a combination of a high level electronic structure calculation within the harmonic approximation with a path integral anharmonicity correction using a lower level method.

## I. INTRODUCTION

After solving the electronic structure problem, most molecular modeling simulations treat nuclei as classical particles. While this often is an appropriate point of view, it fails completely in some cases, and almost always when hydrogen is involved in bond breaking or formation. Strong nuclear quantum effects have been observed in many reactions and recently even in several enzymatic reactions [1–3]. In such situations, one should treat some or all nuclei quantum mechanically. In particular, the nuclear quantum effects should be considered in the simulation even though they may be similar for the corresponding reactions in enzyme and in solution, and therefore may not contribute to the catalytic effect of the enzyme [4, 5].

Solving the time-dependent Schrödinger equation exactly is of course possible only for a handful of atoms [6]. Luckily, in most chemical reactions, some quantum effects are at least partially washed out by finite temperature. Whereas the "real-time" quantum dynamics is extremely difficult, quantum thermodynamics, or "imaginary-time" quantum dynamics, can be computed accurately for fairly large systems using the Feynman path integrals [7, 8].

In general physics, path integrals are mostly known as an elegant tool to formulate analytical theories in particle physics and quantum field theory. In chemical physics, the somewhat abstract path integrals have evolved into an extremely practical numerical tool [9, 10]. In fact, they are probably the most successful tool in solving quantum statistical problems in large systems without symmetry.

In this paper, we describe how path integrals can be used to compute the equilibrium isotope effects, kinetic isotope effects, and the temperature dependence of the reaction rate constant.

## II. METHODOLOGY

### A. Path integral methods

The central quantity in quantum statistical mechanics is the partition function,

$$Q(\beta) = \sum_n e^{-\beta \varepsilon_n} \tag{1}$$

where $\beta = (k_B T)^{-1}$ is the inverse temperature and $\varepsilon_n$ is the energy of the system in the eigenstate $n$. If the partition function is known analytically, any thermodynamic quantity can be found. E.g., the thermal energy can be computed as

$$E = -\frac{\partial \ln Q(\beta)}{\partial \beta}. \tag{2}$$

The beauty of path integrals lies in that they allow computing the partition function without finding the eigenstates of the Hamiltonian. Let us therefore consider a molecular system consisting of $N$ atoms with masses $m_i$. Starting from the exact expression $Q(\beta) = \text{Tr}(e^{-\beta \hat{H}})$, one obtains the path integral (PI) representation of $Q$ as $Q = \lim_{P \to \infty} Q_P$, with [10]

$$Q_P(\beta) = C \int d\mathbf{r}^{(1)} \cdots \int d\mathbf{r}^{(P)} \exp\left[-\beta \Phi\left(\left\{\mathbf{r}^{(s)}\right\}\right)\right]. \tag{3}$$

Above, $C \equiv \left(\frac{P}{2\pi\hbar^2\beta}\right)^{3NP/2} \prod_{i=1}^{N} m_i^{3P/2}$ is a multiplicative factor, $P$ the number of imaginary time slices, and

*Electronic address: jiri.vanicek@epfl.ch

$\mathbf{r}^{(s)} \equiv (\mathbf{r}_1^{(s)}, \mathbf{r}_2^{(s)}, \ldots, \mathbf{r}_N^{(s)})$ the set of Cartesian coordinates associated with the $s$th time slice. Finally, $\Phi\left(\{\mathbf{r}^{(s)}\}\right)$ is the effective potential given by

$$\Phi\left(\{\mathbf{r}^{(s)}\}\right) = \frac{P}{2\hbar^2\beta^2} \sum_{s=1}^{P} \sum_{i=1}^{N} m_i \left(\mathbf{r}_i^{(s)} - \mathbf{r}_i^{(s-1)}\right)^2$$
$$+ \frac{1}{P} \sum_{s=1}^{P} V\left(\mathbf{r}^{(s)}\right) \quad (4)$$

with $\mathbf{r}^{(0)} \equiv \mathbf{r}^{(P)}$ and $\{\mathbf{r}^{(s)}\}$ representing $\{\mathbf{r}^{(1)}, \mathbf{r}^{(2)}, \ldots, \mathbf{r}^{(P)}\}$.

From expressions (3) and (4) it is obvious that for $P = 1$ one obtains the classical partition function and therefore classical thermodynamics. The quantum thermodynamics is obtained in the limit $P \to \infty$, but in practice it often suffices to take a finite value of $P$ to obtain accurate quantum results.

To compute a thermal average $A(\beta)$ of a physical observable $A$ such as the heat capacity or a rate constant, one starts from the exact quantum expression $A(\beta) = \text{Tr}[\hat{A}\exp(-\beta\hat{H})]/Q(\beta)$ or, if possible, from an exact expression for $A(\beta)$ in terms of the partition function, such as Eq. (2) for energy. Using the PI expression (3) for $Q$, one ends up with a PI expression for the thermal average $A(\beta)$,

$$A(\beta) = \left\langle A\left(\{\mathbf{r}^{(s)}\}\right)\right\rangle_\rho, \quad (5)$$

where $\langle\cdot\rangle_\rho$ denotes a weighted average over PI integral configurations. The weight is given by $\rho = \exp(-\beta\Phi)$ and the quantity $A\left(\{\mathbf{r}^{(s)}\}\right)$ is called a PI "estimator" for $A(\beta)$.

The PI average (5) can be evaluated efficiently using a PI molecular dynamics (PIMD) or PI Monte Carlo (PIMC) techniques [10]. In the calculations presented below, a PIMD implementation in the molecular dynamics package AMBER 10 [11] was used for the equilibrium isotope effects while an in-house PIMC code was used for the kinetic isotope effects and the temperature dependence of the rate constant.

Up to this point, everything was straightforward. The interesting twist comes because the estimator $A\left(\{\mathbf{r}^{(s)}\}\right)$ is not a unique function of $\{\mathbf{r}^{(s)}\}$. The art of PIs lies in finding the optimal estimator in the sense of having the smallest statistical error for a given number $M$ of samples. As the statistical error of a simulation is proportional to $M^{-1/2}$, an estimator with a smaller statistical error can lead to a much more efficient simulation.

## B.  Equilibrium isotope effects

The first application that we shall consider is the calculation of the equilibrium isotope effect (EIE), defined as the effect of isotopic substitution on the equilibrium constant. More precisely,

$$\text{EIE} = \frac{K_l}{K_h}, \quad (6)$$

where $K$ is the equilibrium constant and $l$ $(h)$ denotes the lighter (heavier) isotope. The equilibrium constant can be expressed in terms of partition functions as $K = Q_p/Q_r$ where subscripts $p$ and $r$ denote the product and reactant, respectively. Hence the EIE can be computed as

$$\text{EIE} = \frac{\exp\left[-\beta \int_0^1 d\lambda \frac{dF_p(\lambda)}{d\lambda}\right]}{\exp\left[-\beta \int_0^1 d\lambda \frac{dF_r(\lambda)}{d\lambda}\right]}, \quad (7)$$

where $F = -\beta^{-1}\log Q$ is the free energy and $\lambda$ is a parameter providing a smooth transition between the lighter and heavier isotopologs [12]. For instance, it can be accomplished by a linear interpolation of masses of all atoms in a molecule according to the equation

$$m_i(\lambda) = (1-\lambda)\,m_{h,i} + \lambda m_{l,i}. \quad (8)$$

Unlike the partition function or the equilibrium constant $K$, the derivative $dF/d\lambda$ of the free energy can be computed by a PIMD or PIMC simulation directly, and so the equilibrium constant can be computed by the so-called thermodynamic integration (TI) expressed in Eq. (7). The estimator for $dF/d\lambda$ can be found in Ref. 12.

## C.  Quantum instanton approximation

Theoretically more challenging quantities than the equilibrium constant or EIE are the rate constant or the kinetic isotope effect (KIE). The reason is that these kinetic quantities combine quantum thermodynamics with the real-time quantum dynamics. However, since the most interesting chemical reactions occur at a thermodynamically relatively high temperature, there exist suitable approximations.

A recent and accurate approximation which takes into account most quantum effects is the so-called quantum instanton (QI) approximation of Miller and coworkers [13]. In this approximation, the rate constant is expressed as

$$k_{\text{QI}}(\beta) = \frac{\sqrt{\pi}}{2} \frac{\hbar}{\Delta H} \frac{C_{\text{ff}}(0)}{Q_r}, \quad (9)$$

where $C_{\text{ff}}(t)$ is the flux-flux correlation function, $Q_r$ the reactant partition function, and $\Delta H$ a certain energy variance near the transition state.

## D.  Kinetic isotope effects

The kinetic isotope effect is defined as the effect of isotopic substitution on the rate constant,

$$\text{KIE} = \frac{k_l}{k_h}. \quad (10)$$

This KIE is widely used in chemical kinetics to detect nuclear tunneling and other quantum effects, as well as to distinguish between possible reaction mechanisms. Unlike the rate constant itself, the KIE depends very little on the classical energy barrier height, and so the KIE can separate various effects from the simple exponential dependence on the barrier that overwhelms the rate constant. Using the QI expression (9), the KIE can be expressed as [14]

$$\text{KIE} = \frac{Q_{r,h}}{Q_{r,l}} \frac{\Delta H_h}{\Delta H_l} \frac{C_{\text{dd},l}(0)}{C_{\text{dd},h}(0)} \frac{\frac{C_{\text{ff},l}(0)}{C_{\text{dd},l}(0)}}{\frac{C_{\text{ff},h}(0)}{C_{\text{dd},h}(0)}}, \qquad (11)$$

where the delta-delta correlation function $C_{\text{dd}}(t)$ was introduced. This correlation function at time $t = 0$ is a generalization of the partition function, constrained to two dividing surfaces. Introduction of $C_{\text{dd}}$ into expression (11) simplifies the calculation: On one hand, similarly to $\Delta H$ the flux factor $C_{\text{ff}}(0)/C_{\text{dd}}(0)$ can be computed directly in a single PIMC or PIMD simulation [15]. On the other hand, the ratio $C_{\text{dd},l}(0)/C_{\text{dd},h}(0)$ can be computed by a TI analogous to Eq. (7). The estimators can be found in Refs. 14, 16, 17.

It should be noted that several other PI approaches to compute the KIE exist, which are however not based on the QI. These include, e.g., approaches based on other quantum transition state theories [18, 19] or on the quantized classical path method [5, 20, 21].

### E. Temperature dependence of the rate constant

The last application that we shall consider is the direct evaluation of the temperature dependence of the rate constant, i.e., of the ratio $k(T)/k(T_0)$. Again, this quantity is extremely useful in kinetics because it can help to discern between plausible mechanisms of a reaction and because the ratio is easier to measure accurately than the rate constant itself.

In the framework of the QI approximation, the $T$ dependence can be evaluated as [22]

$$\frac{k_{\text{QI}}(\beta)}{k_{\text{QI}}(\beta_0)} = \frac{Q_r(\beta_0)}{Q_r(\beta)} \frac{\Delta H(\beta_0)}{\Delta H(\beta)} \frac{C_{\text{dd}}(\beta)}{C_{\text{dd}}(\beta_0)} \frac{\frac{C_{\text{ff}}(\beta)}{C_{\text{dd}}(\beta)}}{\frac{C_{\text{ff}}(\beta_0)}{C_{\text{dd}}(\beta_0)}}. \qquad (12)$$

The flux and energy variance are computed as for the KIEs, but the ratios of the partition functions and of the delta-delta correlation functions use a different type of TI, namely a TI with respect to the inverse temperature $\beta$ [22, 23]. Taking advantage of the relations

$$E_r(\beta) = -\frac{d \log Q_r(\beta)}{d\beta} \text{ and} \qquad (13)$$

$$E^{\ddagger}(\beta) = -\frac{d \log C_{\text{dd}}(\beta)}{d\beta} \qquad (14)$$

between the reactant and transition state energies and the logarithmic derivatives of $Q_r$ and $C_{\text{dd}}$, one can compute the ratios of $Q$s and $C_{\text{dd}}$s as

$$\frac{Q_r(\beta)}{Q_r(\beta_0)} = \exp\left[-\int_{\beta_0}^{\beta} E_r(\tilde{\beta})d\tilde{\beta}\right], \qquad (15)$$

$$\frac{C_{\text{dd}}(\beta)}{C_{\text{dd}}(\beta_0)} = \exp\left[-\int_{\beta_0}^{\beta} E^{\ddagger}(\tilde{\beta})d\tilde{\beta}\right]. \qquad (16)$$

The estimators for the reactant energy $E_r$ are well-known for PIMD simulations [24–26]. Estimators for the transition state energy $E^{\ddagger}$ were developed in Ref. 22 for several types of constraints. These estimators are derived in a similar manner, based on the rescaling of coordinates and a finite difference evaluation of the derivative with respect to $\beta$ that was used for the first time by Predescu and coworkers for reactant energies and heat capacities [27]. The statistical error of these estimators showed a surprising behavior in comparison with the estimators for $E_r$. In particular, the centroid virial estimators was not always the optimal estimator [22]. Below we use estimators from Ref. 22 for both $E_r$ and $E^{\ddagger}$ because they are suitable for a PIMC simulation.

### III. COMPUTATIONAL DETAILS

#### A. Equilibrium isotope effects

To compute the EIE, ratios of partition functions corresponding to different isotopologs of reactants and products have to be computed. Unfortunately, higher level *ab initio* electronic structure methods are usually too expensive to be used in the PI calculation directly. On the other hand, semiempirical or force field methods generally do not achieve comparable accuracy. To take advantage of both the accuracy of *ab initio* methods and the rigor of PI treatment of nuclear motion, we combine the value of the EIE obtained in the harmonic approximation (HA) using a higher level method with the anharmonicity correction, rigorously computed with the PIMD method, using a lower level method. The anharmonicity correction is calculated as

$$\Delta\Delta F^{\text{anharm}} = \Delta F_{\text{PI}}^{\text{red}} - \Delta F_{\text{HA}}^{\text{red}}, \qquad (17)$$

where $\Delta F_{\text{PI}}^{\text{red}}$ and $\Delta F_{\text{HA}}^{\text{red}}$ are the free energy differences computed with the PI method and the HA, respectively. The HA value of $\Delta F^{\text{red}}$ is obtained by Boltzmann averaging over all possible distinguishable conformations,

$$\Delta F_{\text{HA}}^{\text{red}} = -k_B T \ln\left[\frac{s_r \sum_{i=1}^{N_p}\left\{\exp\left(\frac{-E_i^{\text{el}}}{k_B T}\right)\sum_{j=1}^{s_p} Q_{p,ij}^{\text{nuc}}\right\}}{s_p \sum_{i=1}^{N_r}\left\{\exp\left(\frac{-E_i^{\text{el}}}{k_B T}\right)\sum_{j=1}^{s_r} Q_{r,ij}^{\text{nuc}}\right\}}\right], \qquad (18)$$

where $N_r$ is the number of "geometrically different isomers" of the reactant. By geometrically different isomers we mean species differing in their geometry, not

species differing only in positions of isotopically substituted atoms. $E_i^{el}$ is the electronic energy (including nuclear repulsion) of the $i^{th}$ isomer, $s_r$ is the symmetry factor, which can arise from the change of the wave function due to the effects of indistinguishability of particles during isotopic substitution. Finally, $Q_{r,ij}^{nuc}$ are partition functions of the nuclear motion of $s_r$ isotopomers. $N_p$, $s_p$, $Q_{p,ij}^{nuc}$ denote analogous quantities for the product.

Since in our approximation the electronic function does not change after isotopic substitution, the EIE is dominated by vibrational contributions. Therefore, we searched for an optimal electronic structure method among those studied by Merrick *et al.* [28], who tested the performance of several higher level methods by comparison of the computed vibrational frequencies in the HA with experimental data for a set of 39 molecules. The B98/6-311+(2df,p) method, which we chose, has the root mean square error (RMSE) of the zero point energy (ZPE) equal to 0.31 kJ·mol$^{-1}$ and RMSEs of frequencies 31 cm$^{-1}$. The lower level method used to compute the PI anharmonicity corrections was the AM1 semiempirical method [29], which, in the HA, reproduces the B98/6-311+(2df,p) results very well.

Since the value of the EIE is expected to be close to unity, we have chosen a relatively high number of time slices $P = 40$ in the discretized path integral. The TI was performed with Simpson's rule using five values of $\lambda$. As the dependence of the PIMD average of $dF/d\lambda$ is almost linear over the full range of $\lambda$, five points were sufficient to get a converged result for the integral. For further details about the method, see Ref. 12.

## B.   Kinetic isotope effects

The ratio of partition functions needed for the KIE was computed in the same manner as the ratio for the EIE, with the exception that the number of imaginary time slices was set to $P = 24$. Other terms in the Eq. (11) were computed with the PIMC method using the empirical valence bond (EVB) potential [30, 31], which allows the molecular mechanics potential to be fitted to match the B98/6-311+(2df,p) reaction barrier and Hessian at the transition state [32].

The EVB potential is computed as

$$V_{EVB} = \frac{1}{2}\left(V_{11} + V_{22}\right) - \sqrt{|V_{12}|^2 + \left(\frac{V_{11} - V_{22}}{2}\right)^2} \quad (19)$$

where $V_{11}$ and $V_{22}$ are the molecular mechanics potential energies of the reactant and product, respectively. These are the diabatic potentials and the diagonal terms in the symmetric $2 \times 2$ EVB matrix. In our calculations, they were obtained with the general AMBER force field (GAFF) [33]. The off-diagonal term $V_{12}$, i.e., the coupling between the two diabatic states, was calculated according to the formula of Schlegel and Sonnenberg [34]:

$$V_{12}(\mathbf{r}) = A[1 + \mathbf{B}\cdot\Delta\mathbf{r} + \Delta\mathbf{r}\cdot(\mathbf{C} + \alpha\mathbf{I})\cdot\Delta\mathbf{r}]\exp(-\alpha|\Delta\mathbf{r}|^2/2). \quad (20)$$

The constants $A$, $\mathbf{B}$, and $\mathbf{C}$ are chosen to match the barrier height and the Hessian of the *ab initio* potential at the transition state.

## C.   Temperature dependence of the rate constant

A similar procedure as for the KIE was used to compute the temperature dependence of the rate constant. Since the major contribution to the temperature dependence of the rate constant is due to the reaction barrier height, we computed the barrier height also by the single point coupled clusters CCSD(T)/cc-pVTZ and CCSD/aug-cc-pVTZ calculations on B98/6-311+(2df,p) geometries.

In the PI calculation of the temperature dependence of the rate constant, several approaches were used to compute the ratio of reactant partition functions at different temperatures. In the first approach, denoted "QI GAFF(PIMC)", the ratio of the reactant partition functions was computed directly in the PIMC simulation with the GAFF force field. This could possibly cause a difficulty because in the EVB method, the Hessian of potential energy surface at the transition state is fitted to the much more accurate B98/6-311+(2df,p) Hessian. At this point, the fitted surface has B98/6-311+(2df,p) properties in the HA, with the anharmonicity given by a nonlinear combination of the GAFF force fields describing the reactant and product. Therefore, a systematic error could arise due to the different properties of the B98 and GAFF surfaces in the HA. Fortunately, the harmonic vibrational free energy computed using the GAFF force field is only about 0.5 kcal/mol lower than the B98/6-311+(2df,p) value. Consequently, the results obtained with the QI GAFF(PIMC) method are almost equal to the "QI B98(HA) GAFF(PIMC) anharm." results, obtained by augmenting the B98/6-311+(2df,p) free energies in the HA with the anharmonicity PIMC correction computed with the GAFF force field. The "QI B98(HA)" method uses only plain B98/6-311+(2df,p) free energies in the HA. Finally, probably the most accurate "QI B98(HA) AM1(PIMC) anharm." method uses the B98/6-311+(2df,p) free energies in the HA with the anharmonicity PIMC correction computed with the AM1 semiempirical potential.

## Used software

All PIMD calculations were performed in Amber 10 [11]. The *ab initio* and B98 calculations as well as AM1 semiempirical calculations in the HA were done in Gaussian 03 revision E01 [35]. All PIMC calculations were done using a PIMC code developed by one of us.
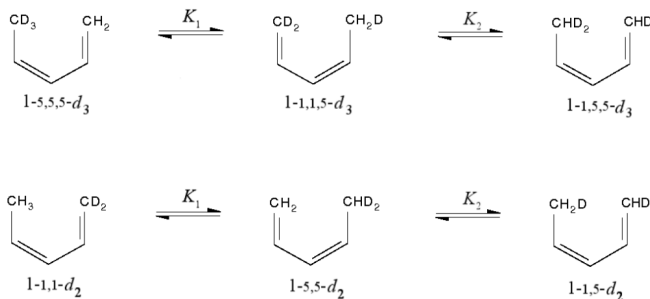
FIG. 1: The [1,5] hydrogen shift reaction in $(3Z)$-$(5,5,5$-$^2H_3)$penta-1,3-diene (**1-5,5,5-$d_3$**) and in $(3Z)$-$(1,1$-$^2H_2)$penta-1,3-diene (**1-1,1-$d_2$**). If all contributions except for those due to symmetry factors were neglected, one would obtain approximate equilibrium constants $K_1 = 3$ for the first reaction step and $K_2 = 2$ for the second step (in both cases).

## IV.   RESULTS

In this section, the path integral formalism is applied to study the [1,5] sigmatropic hydrogen shift reaction in the $(3Z)$-penta-1,3-diene. Two isotopologs of $(3Z)$-penta-1,3-diene are considered: tri-deuterated $(3Z)$-$(5,5,5$-$^2H_3)$penta-1,3-diene (**1-5,5,5-$d_3$**) and di-deuterated $(3Z)$-$(1,1$-$^2H_2)$penta-1,3-diene (**1-1,1-$d_2$**) (see Fig. 1). Both isotopologs were used by Roth and König in their experimental study of the KIE in the [1,5] sigmatropic hydrogen shift reaction [36]. The value of the KIE obtained by Roth and König was too high to be explained classically implying that quantum effects such as tunneling are important in this reaction. Here, we examine both the EIE and KIE for this reaction as well as the temperature dependence of the rate constant in the range studied in the experimental work [36].

### A.   Equilibrium isotope effects

The EIE for both steps of the [1,5] sigmatropic hydrogen shift reaction is computed according to the Eq. (7) and listed in Table I. We have already computed the equilibrium ratios for both isotopologs in Ref. 12. For the convenience of the reader, Table I also shows these ratios.

The precision of the experimental ratios of Roth and König is only to a single significant digit, so it reflects only the ratios caused by the symmetry effects and does not allow for a rigorous comparison with the computed EIE. Nevertheless, in Ref. 12 we were able to use the same methodology to compare the theoretical and experimental equilibrium ratios for a related compound (2,4,6,7,9-pentamethyl-5-methylene-11,11a-dihydro-12$H$-naphthacene). As the experimental data of Doering *et al.* [37] were more accurate, a more rigorous test was possible, and led to the conclusion that the current methodology can reproduce quantitatively
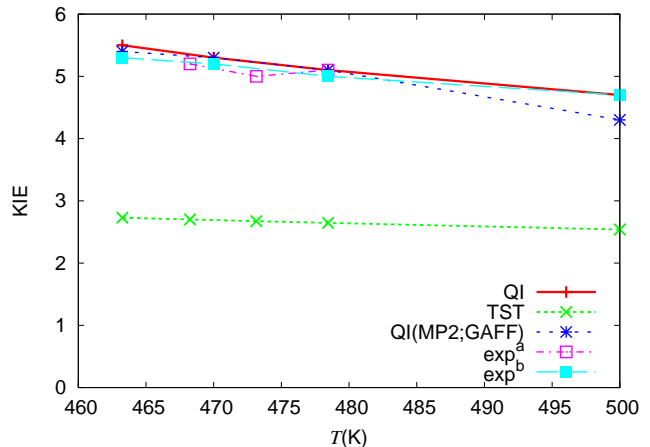


FIG. 2: The KIE on the first [1,5] hydrogen shift reaction from Fig. 1. The displayed KIE is defined precisely in Eq. (21) of the text. The curve marked as exp[a] denotes the raw experimental data from Ref. 36 whereas exp[b] denotes the data computed from an Arrhenius fit in Ref. 36.

the equilibrium ratios beyond the symmetry effects. The value of the EIE for the first reaction step is greater than unity, meaning that the equilibrium of the first step reaction is shifted toward the product side for the lighter isotopolog **1-1,1-$d_2$** (where hydrogen is transferred) in comparison with the heavier **1-5,5,5-$d_3$** (where the transferred atom is deuterium). In the second step, the EIE is smaller than unity so the products are favored for the heavier isotopolog. Also, in contrast to the first step, hydrogen is transferred in the heavier isotopolog and deuterium in the lighter one.

### B.   Kinetic isotope effects

Computed values of the KIE on the first reaction step are shown in Figure 2 and Table II. This KIE is defined as the ratio

$$\text{KIE} = \frac{k(\textbf{1-1,1-}d_2 \rightarrow \textbf{1-5,5-}d_2)}{k(\textbf{1-5,5,5-}d_3 \rightarrow \textbf{1-1,1,5-}d_3)}. \tag{21}$$

As can be seen from the table, the calculated and experimental data agree very well; the largest relative difference is around 5 %. Comparison with the transition state theory (TST) values, computed using the B98/6-311+(2df,p) barrier height and the partition functions in the HA [for reactants computed according to Eq. (18)], clearly demonstrates the importance of quantum effects on the KIE. (Note that in TST the value of the KIE is actually independent of the barrier height). The third column of the table contains the KIE computed in Ref. 17, where the same PI method was used, but the barrier height and the Hessian of the transition state were fitted to MP2/6-31g(d) ab initio data. In addition, the GAFF force field [33] was used not only for the EVB potential

| EIE | | $EIE_1 = K_1(\boldsymbol{d_2})/K_1(\boldsymbol{d_3})$ | $EIE_2 = K_2(\boldsymbol{d_2})/K_2(\boldsymbol{d_3})$ |
|---|---|---|---|
| AM1 (PIMD) | | 1.07 | 0.96 |
| B98 (HA) +AM1 (PIMD) anharm. | | 1.12 | 0.95 |
| Equilibrium fraction | **1-5,5,5-$d_3$** | **1-1,1,5-$d_3$** | **1-1,5,5-$d_3$** |
| AM1 (PIMD) | 0.103 | 0.296 | 0.601 |
| B98 (HA) + AM1 (PIMD) anharm. | 0.104 | 0.293 | 0.602 |
| Equilibrium fraction | **1-1,1-$d_2$** | **1-5,5-$d_2$** | **1-1,5-$d_2$** |
| AM1 (PIMD) | 0.099 | 0.305 | 0.597 |
| B98 (HA) +AM1 (PIMD) anharm. | 0.097 | 0.307 | 0.596 |

TABLE I: Values of the EIE on the first ($K_1$) and second ($K_2$) step of the reactions from Fig. 1 at 478.45 K. Results denoted by AM1 (PIMD) were obtained with a PIMD calculation using the AM1 semiempirical method. Results denoted by B98 (HA) + AM1 (PIMD) anharm. were obtained using the B98 method in the harmonic approximation together with the anharmonicity correction computed with the AM1 method. For reference, the bottom six rows show the equilibrium fractions of all isotopomers occurring in the reactions from Fig. 1.

| $T$ (K) | QI | TST | QI/MP2;GAFF | exp[a] | exp[b] |
|---|---|---|---|---|---|
| 463.25 | 5.5 | 2.7 | 5.4 | - | 5.3 |
| 468.25 | - | 2.7 | - | 5.2 | - |
| 470.0 | 5.3 | 2.7 | 5.3 | - | 5.2 |
| 473.15 | - | 2.6 | - | 5.0 | - |
| 478.45 | 5.1 | 2.6 | 5.1 | 5.1 | 5.0 |
| 500.0 | 4.7 | 2.5 | 4.3 | - | 4.7 |

[a]Ref. 36
[b]Ref. 36

TABLE II: The KIE on the first [1,5] hydrogen shift reaction from Fig. 1. The displayed KIE is defined precisely in Eq. (21) of the text. The column denoted by exp[a] contains the raw experimental data from Ref. 36 whereas the column exp[b] contains the data computed from an Arrhenius fit in Ref. 36.

but also for the reactant partition functions. Our results and results from Ref. 17 differ by at most 10% of the KIE value. The main improvement in comparison with Ref. 17 occurs at higher temperatures. However, the observed difference is not only due to the use of different methods, but partially also due to the way the EVB potential surface is constructed. As discussed in Ref. 17, the results are weakly dependent on the value of $\alpha$ in Eq. (20), and even though a flat plateau is obtained for a broad range of $\alpha$ values, varying $\alpha$ still can change the KIE by about 10%. Generally, the optimal value of the parameter $\alpha$ can be different for different *ab initio* methods. Here we have intentionally chosen the same value of $\alpha = 0.9$ as in Ref. 17. As the final results are still fairly close and both agree well with the experimental value, this demonstrates the relative robustness of the method once a proper value of $\alpha$ is chosen. In order to achieve an even higher accuracy and to remove a certain level of arbitrariness connected with the parameter $\alpha$, one can use, e.g., the distributed gaussian method [34]. In this method, the EVB potential is fitted to match the Hessian of an *ab initio* potential at several points in the transition state region.

## C. Temperature dependence of the rate constant

In contrast to the KIE which is virtually independent of the barrier height, the rate constant depends on the barrier height exponentially. Very accurate value of the barrier height is therefore essential for the calculation of this quantity or its temperature dependence. Table III contains barrier heights, relative energies of trans and gauche isomers of $(3Z)$-penta-1,3-diene, and TST values of the rate constant $k_{d_2}^{\mathrm{TST}}$ for the **1-1,1-$d_2$ $\rightarrow$ 1-5,5-$d_2$**, hydrogen shift computed at three different levels of theory using B98/6-311+(2df,p) optimized geometries. As can be seen from the table, the B98/6-311+(2df,p) barrier is the lowest one, in accordance with the well known fact that barrier heights are usually underestimated by the majority of currently used density functional methods (including B98) [38]. Besides B98, two other and generally more accurate methods used were the CCSD(T) method with the cc-pVTZ basis set and the CCSD method without triples correction but with the substantially larger aug-cc-pVTZ basis set. The difference between these two methods is still almost 3 kcal/mol but at this point it is hard to decide which method is actually closer to the real value of the barrier.

The TST rate constants listed in Table III were computed using the B98/6-311+(2df,p) partition functions in the HA together with the barrier height of the method considered. Neglecting the effect of barrier recrossing and the anharmonicity of the potential energy surface, the TST rate constant should be smaller than the experimental one, because the TST ignores the tunneling contribution that is quite important in this reaction (as demonstrated by the large value of the KIE). As a consequence, comparison of $k_{d_2}^{\mathrm{TST}}$ with the experimental rate constant suggests that both the CCSD(T)/cc-pVTZ and especially the B98/6-311+(2df,p) methods give too low barriers. The TST rate constant computed with the CCSD/aug-cc-pVTZ barrier, on the other hand, agrees quite well with the theoretical expectations.

The QI method provides several theoretical improve-

| | B98/6-311+(2df,p) | CCSD(T)/cc-pVTZ | CCSD/aug-cc-pVTZ | exp[a] |
|---|---|---|---|---|
| $\Delta\varepsilon^{\ddagger}$(kcal/mol) | 37.3 | 39.9 | 42.8 | |
| $\Delta\varepsilon^{g-t}$(kcal/mol) | 3.6 | 3.0 | 2.0 | |
| $k_{d_2}^{\text{TST}} \cdot 10^{-6}(s^{-1})$[478.45 K] | 364.6 | 27.8 | 2.8 | 7.1 |

[a]Ref. 36

TABLE III: The barrier height $\Delta\varepsilon^{\ddagger} = \varepsilon^{\ddagger} - \varepsilon_r^{\text{trans}}$ measured from the trans conformer $(3Z)$-penta-1,3-diene which is the global minimum, the energy difference $\Delta\varepsilon^{g-t} = \varepsilon_r^{\text{gauche}} - \varepsilon_r^{\text{trans}}$ between trans and gauche conformers, and the TST rate constant $k_{d_2}^{\text{TST}}$ of the [1,5] hydrogen shift reaction **1-1,1-$d_2$ → 1-5,5-$d_2$**.



FIG. 3: Temperature dependence of the rate constant of the [1,5] hydrogen shift reaction **1-1,1-$d_2$ → 1-5,5-$d_2$** using the CCSD/aug-cc-pVTZ barrier height. The $y$ axis is plotted in the logarithmic scale. The description of methods used can be found in Computational details.

ments over the TST: Most importantly, unlike the TST, the QI approximation includes tunneling and other quantum effects. Moreover, its PI implementation facilitates the calculation of the anharmonicity effects on the partition functions and delta-delta correlation functions. Methods used to include the anharmonicity correction to the B98/6-311+(2df,p) harmonic ratios are described in the Computational details. The temperature dependence of the QI rate constant with the CCSD/aug-cc-pVTZ barrier is shown in Figure 3.

As can be seen in Figure 3, both the QI and TST results agree well with the relatively broad and imprecise experimental temperature dependence. Neglecting again the recrossing and anharmonicity effects, one can expect that the value of $k_{d_2}^{\text{TST}}$ will be smaller than the value of $k_{d_2}^{\text{QI}}$, mainly due to the tunneling contribution to the rate that is captured by $k_{d_2}^{\text{QI}}$ but ignored in $k_{d_2}^{\text{TST}}$. Moreover, as the relative importance of the tunneling increases with the decreasing temperature, the temperature dependence of the $k_{d_2}^{\text{QI}}$ should be weaker than the dependence of $k_{d_2}^{\text{TST}}$. Figure 3 shows that this is indeed true. (The temperature dependence of the relative importance of tunneling and of other nuclear quantum effects can be sometimes more complicated due to other effects such as the tem-

perature dependence of the distance between the donor and acceptor [21].)

Another interesting feature visible in the graph is the importance of the anharmonicity correction, which shows that the change in the temperature dependence caused by the anharmonicity can be equivalent to the change of the reaction barrier by several kcal/mol. It is reassuring that the more accurate AM1 correction influences the result more than the correction computed using the GAFF force field. This observation agrees well with the expectations based on the fact that in the GAFF force field the bond stretching coordinates are actually harmonic and the anharmonicity is caused only by the other terms of the force field. Nevertheless, both corrections decrease the HA free energy of nuclear motion through the lowering of the ZPE. Finally, the curves of the relative rate constant in the Arrhenius plot are almost exactly straight lines, irrespective of the theoretical method used. This suggests that it would be very hard to observe any non-Arrhenius behavior in this small temperature range even with a far more precise experimental setup.

The temperature dependence of $k_{d_2}$ computed with the CCSD(T)/cc-pVTZ barrier height is shown in Figure 4. With this barrier, the temperature dependence of the more accurate QI method is only very slightly weaker than the experimental dependence, whereas the TST rate dependence is still within the range of the experimental values. However, this apparently excellent agreement of the conventional TST with the experiment is most likely due to the cancellation of the tunneling and anharmonicity corrections. All the other characteristics of the graph are the same as with the CCSD/aug-cc-pVTZ barrier. When the lowest and probably the least accurate B98/6-311+(2df,p) barrier is used, curves for all methods stay above the experimental data in the Arrhenius plot.

## V. CONCLUSIONS

We have applied a general path integral methodology for computing the EIE, KIE, and the temperature dependence of the rate constant to the [1,5] sigmatropic hydrogen shift in pentadiene. In case of the EIE, the computed result has a higher precision than the experiment [36], therefore our result can be considered as a prediction of the deviation of the exact EIE from the symmetry determined EIE. In case of the KIE, the accuracy of the previ-
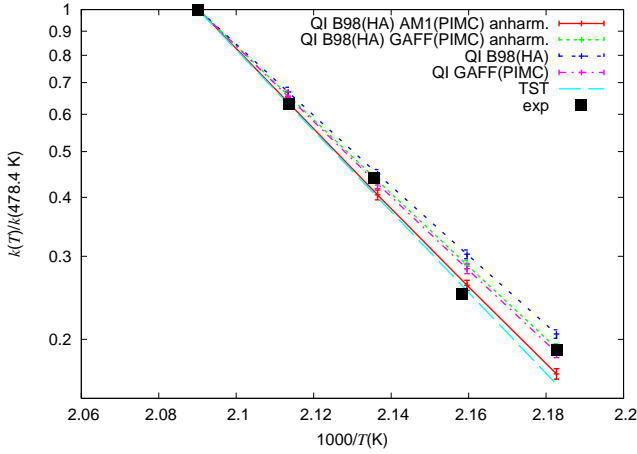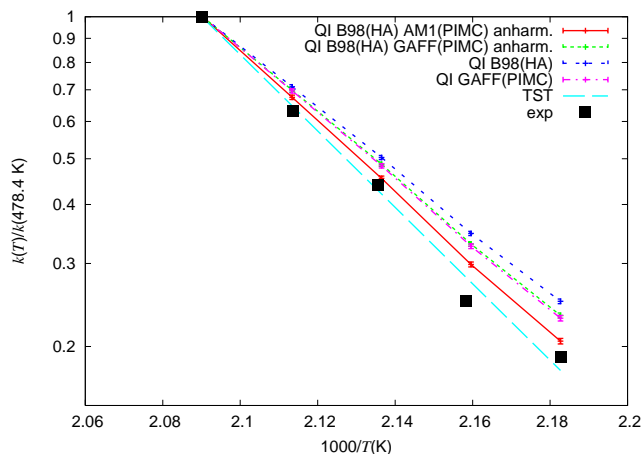
FIG. 4: Temperature dependence of the rate constant of the [1,5] hydrogen shift reaction **1-1,1-$d_2$** $\rightarrow$ **1-5,5-$d_2$** using the CCSD(T)/cc-pVTZ barrier height. The $y$ axis is plotted in the logarithmic scale. The description of methods used can be found in Computational details.

ous result [17] was improved by using a combination of a high level electronic structure calculation within the harmonic approximation with a path integral anharmonicity correction using a lower level method. Finally, the result for the temperature dependence of the rate constant is the first application of the methodology from Ref. 22 to a molecule with more than three atoms. As for the

KIE, the temperature dependence confirms the importance of tunneling and anharmonicity effects. However, unlike for the KIE, the accuracy of the energy barrier plays an important role and therefore a high level method is required. According to our results, the CCSD/aug-cc-pVDZ barrier height of 42.8 kcal/mol seems to be the most accurate.

While we have considered a gas phase molecule with 13 atoms, significantly larger systems can be treated by the presented PI approach since only the light atoms participating in the reaction require a large number $P$ of replicas. Heavier atoms or atoms less important in a given problem (e.g., atoms far from the active site of an enzyme) can be treated either with a small value of $P$ or fully classically (i.e., with $P = 1$). The efficiency will then be dominated by the cost of an accurate potential energy for which various strategies are known already from classical molecular dynamics. Among these are the recent implementations (see, e.g., Ref. 39) of polarizable force fields [40, 41] or the accelerated sampling using hybrid quantum-mechanical/molecular-mechanical potentials [42]. A combination of such techniques with the methodology described in this paper will be the subject of future applications.

### Acknowledgments

[1] A. Kohen, R. Cannio, S. Bartolucci, and J. P. Klinman, Nature **399**, 496 (1999).

[2] J. Basran, M. J. Sutcliffe, and N. S. Scrutton, Biochemistry **38**, 3218 (1999).

[3] L. Masgrau, A. Roujeinikova, L. O. Johanissen, P. Hothi, J. Basran, K. E. Ranaghan, A. J. Mulholland, M. J. Sutcliffe, N. S. Scrutton, and D. Leys, Science **312**, 237 (2006).

[4] K. M. Doll, B. R. Bender, and R. G. Finke, J. Am. Chem. Soc. **125**, 10877 (2003).

[5] M. H. M. Olsson, P. E. M. Siegbahn, and A. Warshel, J. Am. Chem. Soc. **126**, 2820 (2004).

[6] D. C. Clary, Science **321**, 789 (2008).

[7] R. Feynman and A. Hibbs, *Quantum Mechanics and Path Integrals* (McGraw-Hill, 1965).

[8] H. Kleinert, *Path Integrals in Quantum Mechanics, Statistics, Polymer Physics and Financial Markets* (World Scientific Publishing Co. Pte. Ltd., 2004).

[9] B. J. Berne and D. Thirumalai, Annu. Rev. Phys. Chem. **37**, 401 (1986).

[10] D. M. Ceperley, Rev. Mod. Phys. **67**, 279 (1995).

[11] D. A. Case, T. A. Darden, T. E. Cheatham, C. Simmerling, J. Wang, R. Duke, R. Luo, M. Crowley, R.C.Walker, W. Zhang, et al., *Amber 10* (2008), University of California, San Francisco.

[12] T. Zimmermann and J. Vaníček, J. Chem. Phys. **131**, 024111 (2009).

[13] W. H. Miller, Y. Zhao, M. Ceotto, and S. Yang, J. Chem. Phys. **119**, 1329 (2003).

[14] J. Vaníček, W. H. Miller, J. F. Castillo, and F. J. Aoiz, J. Chem. Phys. **123**, 054108 (2005).

[15] T. Yamamoto and W. H. Miller, J. Chem. Phys. **120**, 3086 (2004).

[16] J. Vaníček and W. H. Miller, In *Proceedings of the 8th International Conference: Path Integrals from Quantum Information to Cosmology* ed. C. Burdik, O. Navratil, and S. Posta (JINR, Dubna, 2005).

[17] J. Vaníček and W. H. Miller, J. Chem. Phys. **127**, 114309 (2007).

[18] A. Calhoun and G. A. Voth, J. Phys. Chem. B **102**, 8563 (1998).

[19] R. Iftimie and J. Schofield, Int. J. Quant. Chem. **91**, 404 (2003).

[20] J. K. Hwang, Z. T. Chu, A. Yadav, and A. Warshel, J. Phys. Chem. **95**, 8445 (1991).

[21] H. Liu and A. Warshel, J. Phys. Chem. B **111**, 7852 (2007).

[22] M. Buchowiecki and J. Vaníček, J. Chem. Phys. (2010).

[23] M. Ceotto and W. H. Miller, J. Chem. Phys. **120**, 6356 (2004).

[24] J. A. Barker, J. Chem. Phys. **70**, 2914 (1979).

[25] M. Herman, E. Bruskin, and B. Berne, J. Chem. Phys. **76**, 5150 (1982).

[26] M. Parrinello and A. Rahman, J. Chem. Phys. **80**, 860

(1984).

[27] C. Predescu, D. Sabo, J. D. Doll, and D. L. Freeman, J. Chem. Phys. **119**, 12119 (2003).

[28] J. Merrick, D. Moran, and L. Radom, J. Phys. Chem. A **111**, 11683 (2007).

[29] M. J. S. Dewar, E. G. Zoebisch, E. F. Healy, and J. J. P. Stewart, J. Am. Chem. Soc. **107**, 3902 (1985).

[30] A. Warshel and R. M. Weiss, J. Am. Chem. Soc. **102**, 6218 (1980).

[31] A. Warshel, *Computer Modeling of Chemical Reactions in Enzymes and Solutions* (John Wiley and Sons, New York, 1991).

[32] Y. T. Chang and W. H. Miller, J. Phys. Chem. **94**, 5884 (1990).

[33] J. Wang, R. M. Wolf, J. W. Caldwell, P. Kollman, and D. A. Case, J. Comp. Chem. **25**, 1157 (2004).

[34] H. B. Schlegel and J. L. Sonnenberg, J. Chem. Theory Comput. **2**, 905 (2006).

[35] M. J. Frisch, G. W. Trucks, H. B. Schlegel, G. E. Scuseria, M. A. Robb, J. R. Cheeseman, J. A. Montgomery, Jr., T. Vreven, K. N. Kudin, J. C. Burant, et al., *Gaussian 03, Revision E.01*, Gaussian, Inc., Wallingford, CT, 2004.

[36] W. R. Roth and J. König, J. Liebigs Ann. Chem. **699**, 24 (1966).

[37] W. V. Doering and E. J. Keliher, J. Am. Chem. Soc. **129**, 2488 (2007).

[38] Y. Zhao, N. Gonzalez-Garcia, and D. G. Truhlar, J. Phys. Chem. A **109**, 2012 (2005).

[39] N. Gresh, G. A. Cisneros, T. A. Darden, and J.-P. Piquemal, J. Chem. Theory Comput. **3**, 1960 (2007).

[40] A. Warshel and M. Levitt, J. Mol. Biol. **103**, 227 (1976).

[41] A. Warshel, M. Kato, and A. V. Pisliakov, J. Chem. Theory Comput. **3**, 2034 (2007).

[42] S. C. L. Kamerlin, M. Haranczyk, and A. Warshel, J. Phys. Chem. B **113**, 1253 (2009).